Hindawi
International Journal of Aerospace Engineering
Volume 2019, Article ID 5483073, 12 pages
https://doi.org/10.1155/2019/5483073

Research Article

Dynamical Modelling and Robust Control for an Unmanned Aerial Robot Using Hexarotor with 2-DOF Manipulator

Li Ding[1] **and Hongtao Wu**[2]

[1]*College of Mechanical Engineering, Jiangsu University of Technology, No. 1801 Zhongwu Street, Changzhou, China*
[2]*College of Mechanical and Electrical Engineering, Nanjing University of Aeronautics and Astronautics, No. 29 Yudao Street, Nanjing, China*

Correspondence should be addressed to Li Ding; nuaadli@163.com

Received 6 May 2019; Accepted 9 September 2019; Published 21 October 2019

Academic Editor: Jacopo Serafini

The robust control issues in trajectory tracking of an unmanned aerial robot (UAR) are challenging tasks due to strong parametric uncertainties, large nonlinearities, and high couplings in robot dynamics. This paper investigates the dynamical modelling and robust control of an aerial robot using a hexarotor with a 2-degrees-of-freedom (DOF) manipulator in a complex aerial environment. Firstly, the kinematic model and dynamic model of the aerial robot are developed by the Euler-Lagrange method. Afterwards, a linear active disturbance rejection control is designed for the robot to achieve a high-accuracy trajectory tracking goal under heavy lumped disturbances. In this control scheme, the modelling uncertainties and external disturbances are estimated by a linear extended state observer, and the high tracking precision is guaranteed by a proportion-differentiation (PD) feedback control law. Meanwhile, an artificial intelligence algorithm is applied to adjust the control parameters and ensure that the state variables of the robot converge to the references smoothly. Furthermore, it requires no detailed knowledge of the bounds on unknown dynamical parameters. Lastly, numerical simulations and experiments validate the efficiency and advantages of the proposed method.

1. Introduction

Recently the capability of UARs has been expanded radically with multidegrees-of-freedom aerial manipulators. The most attractive aspect of UARs is that they have enormous potential in interacting with the environment, such as taking samples of material from areas difficult to access, inspection and maintenance of high power lines, and transporting a payload. As a typical nonlinear and coupled system, several works about the UARs have been reported in the literature concerning kinematics and dynamics [1, 2], trajectory planning [3], control [4, 5], and cooperation [6]. In these works, the high-performance manipulation capacity of the UARs depends on an appropriate flight controller. However, the flight controller designers must have a good understanding of a wide range of disciplines, including flight dynamics, robotics, control theory, simulation analysis, and verification and validation. Therefore, it is a challenge for researchers to design a satisfied controller. This paper provides some discussion about the issues in dynamical modelling and robust controller of a UAR using a hexarotor with 2-DOF manipulator.

First of all, the complexity in modelling of UARs mainly arises from the coupled dynamics between the aircraft and the manipulator. For example, the roll inputs can produce pitch responses as large as the pitch responses. Aircraft motion can produce a very large manipulator motion. Hence, the coupling effect may cause a change in the physical parameters of the system during the operating process. Aiming at this issue, the aerial robot is divided into two subsystems, namely, the aircraft and the manipulator. The coupling effect of the two subsystems was regarded as an external disturbance. For example, Orsag et al. [7] had analysed the internal relationship between the manipulator and the aircraft to develop the dynamic models of the two subsystems by the Newton-Euler method. Pounds and Dollar [8] used the Lagrange method to obtain the dynamic model of an aerial

robot, of which the single-DOF manipulator was treated as a variable load. On the contrary, some researchers treated the coupling effect as modelling uncertainties so that an integrated model could be established. For example, Ding and Yu [9] regarded the forces and torques of the manipulator as the total disturbances and considered the entire aerial robot system as a single rigid body to obtain its kinematics and dynamics. Abaunza et al. [10] adopted a dual quaternion method to generate the dynamic model of an aerial robot using a quadrotor with a 3-DOF manipulator. In this paper, the latter scheme is chosen to obtain the dynamic model of an aerial robot using a hexarotor with a 2-DOF manipulator based on the Euler-Lagrange method.

The design of a flight control system is another issue. The applications of UARs strongly depend on the fact that movement of the aircraft is satisfactorily stabilized. Indeed, if the position or attitude of the aircraft is not controlled with high precision, the equipped manipulator will suffer vibration and give up the operating task. Meanwhile, the influence of unknown environment and the interaction among different subsystems have to be carried out. Moreover, the controller design process should seek a method to balance the trade-offs between stability, performance metrics, and robustness to noise and uncertainties. Satisfying external constraints and considering the dynamical nature of the aerial robot system, robust control of the UARs is still an open problem.

The robust control issue can be handled using the following two approaches, termed the model-based approach and the model-free approach. In the former approach, the full information about the aerial robot plant should be known a priori. Accordingly, a subsystem (state observer [11], output observer [12], Kalman's filter [13], etc.) is built, which reconstructs the plant output and rejects the disturbances. These control laws are parameterized based on the known model, such as the linear quadratic control (LQR) [14], model predictive control (MPC) [15], and H_∞ control [16]. It is obvious that constructing these control laws requires continuously updated information about the working model of the plant in the real-time implementation. The aftereffects of any occurring instability are then accommodated using a high gain. In that case, undesirable transients may occur, which causes saturation of actuators and damage to the components in the system. On the other hand, the model-free approach becomes an alternative way to design a control law based on the data of input and output. It is deemed more convenient than the model-based approach, which attracts many researchers to focus on it. For example, a proportional integral derivative (PID) control structure for a quadrotor with lightweight manipulator was discussed in Ref. [17]. The proposed controller could compensate for the reactionary forces during both flight and manipulation. In Ref. [18], Kim et al. proposed an adaptive sliding mode controller (SMC) for a cooperative aerial manipulation to manipulate the pose of the object, which is also verified by simulations and experiments. Jimenez-Cano et al. [2] designed a variable parameter integral backstepping controller for an unmanned helicopter equipped with robotic multilink arms, and the effectiveness of this controller was verified in simulation.

In the aerial control system application, it is also important to suppress the response to lumped disturbances. A good example of this was in the development of a robust control law, where relevant controller design adopted the linear active disturbance rejection control (LADRC) [19–21]. This technique utilizes a linear extended state observer (LESO) to estimate the lumped disturbances and adopts a proportional derivative (PD) control law to ensure convergence of the system output. However, the linear methods cannot afford satisfactory trajectory tracking performance for UARs with high nonlinearity under large motion envelope. The main contributions of this paper are threefold. Firstly, a system model of a UAR including kinematics and dynamics has been established. Secondly, a LADRC is developed for trajectory tracking control of a UAR, where a LESO is used to estimate the disturbances. Meanwhile, an artificial intelligence algorithm called the artificial bee colony (ABC) algorithm is introduced to adjust the control parameters of LADRC. Thirdly, the proposed method is investigated by a series of simulations and experiments. To the best of our knowledge, no reports on robust control using LADRC for the UAR are available until now.

The outline of this paper is arranged as follows. The system modelling of the aerial robot by the Euler-Lagrange method is described in Section 2. In Section 3, a robust control strategy is presented. Stability analysis and parameter tuning of the control system are illustrated in Section 4. Meanwhile, comparative simulations are performed to demonstrate the effectiveness of the proposed controller. An experimental validation with flight tests is provided in Section 5. Finally, some conclusions and contributions are summarized in Section 6.

2. System Description

2.1. Kinematics. As depicted in Figure 1, there are three coordinate frames in the UAR system: the earth-fixed frame $\{I\}$, body-fixed frame $\{B\}$, and manipulator-fixed frame $\{M\}(M = 1, 2, e)$. Let the generalized coordinate of the aerial robot be expressed by

$$\mathbf{q} = \left[\mathbf{p}^T, \Omega^T, \Theta^T\right]^T = [x, y, z, \psi, \theta, \phi, \varepsilon_1, \varepsilon_2]^T \in \mathbb{R}^{8\times 1}, \quad (1)$$

where $\mathbf{p} = [x, y, z]^T$ and $\Omega = [\phi, \theta, \psi]^T$ denote the position and the Euler angles of the hexarotor in the inertial frame, respectively. Furthermore, ϕ is the roll angle, θ is the pitch angle, and ψ is the yaw angle. The vector $\Theta = [\varepsilon_1, \varepsilon_2]^T$ represents the joint angles of the 2-DOF manipulator.

Using the rotation matrix ${}^I\mathbf{R}_B$, the linear velocity ${}^B\dot{\mathbf{P}}$ of the frame $\{B\}$ is written relative to the frame $\{I\}$ as

$$\dot{\mathbf{p}} = {}^I\mathbf{R}_B\, {}^B\dot{\mathbf{p}}. \quad (2)$$

Similarly, let ω denote the angular velocity in the frame $\{I\}$. The angular velocity ${}^B\omega$ of the frame $\{B\}$ is expressed relative to the frame $\{I\}$ as

$$\omega = {}^I\mathbf{R}_B\, {}^B\omega. \quad (3)$$

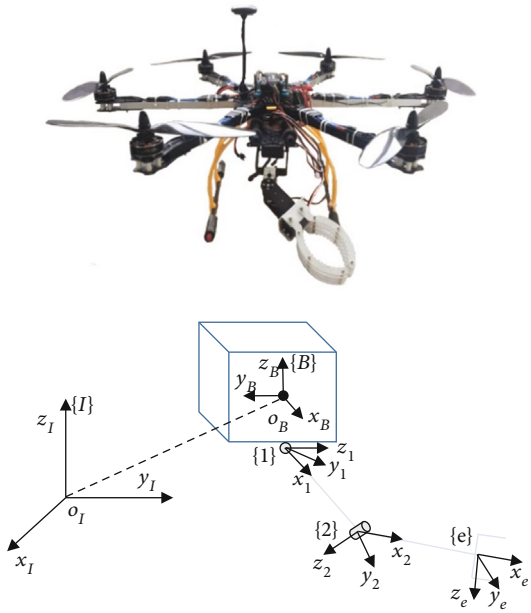

Figure 1: Reference frames and vectors of our UAR.

Besides, the Euler angular rate $\dot{\Omega}$ can be transformed to the angular velocity ω by the standard kinematic relationship:

$$\omega = \mathbf{T}\dot{\Omega}, \tag{4}$$

where $\mathbf{T}$ is the transformation matrix.

Substituting equation (4) to equation (3), one obtains

$${}^{B}\omega = {}^{I}\mathbf{R}_{B}{}^{T}\mathbf{T}\dot{\Omega}. \tag{5}$$

Subsequently, the centre of mass of the link $i(i = 1, 2)$ is computed as

$${}^{I}\mathbf{p}_{i} = {}^{I}\mathbf{R}_{B}\left({}^{B}\mathbf{p} + {}^{B}\mathbf{p}_{i}\right) = \mathbf{p} + {}^{I}\mathbf{R}_{B}{}^{B}\mathbf{p}_{i}. \tag{6}$$

To determine the relationship among the joint velocity ${}^{B}\dot{\mathbf{p}}_{i}$, angular velocity ${}^{B}\omega_{i}$, and end-effector velocity $\dot{\Theta}$, one gets

$$\begin{cases} {}^{B}\dot{\mathbf{p}}_{i} = \mathbf{J}_{P}(\Theta)\dot{\Theta}, \\ {}^{B}\omega_{i} = \mathbf{J}_{O}(\Theta)\dot{\Theta}, \end{cases} \tag{7}$$

where $\mathbf{J}_{P}(\Theta)$ and $\mathbf{J}_{O}(\Theta)$ are the manipulator Jacobian matrix. The calculation of the Jacobian is referred to Ref. [22].

Then, the linear velocity and angular velocity relative to the frame $\{I\}$ are concluded as

$$\begin{cases} {}^{I}\dot{\mathbf{p}}_{i} = \dot{\mathbf{p}} + \mathbf{S}(\omega){}^{I}\mathbf{R}_{B}{}^{B}\mathbf{p}_{i} + {}^{I}\mathbf{R}_{B}\mathbf{J}_{P}(\Theta)\dot{\Theta}, \\ {}^{I}\omega_{i} = \omega + {}^{I}\mathbf{R}_{B}\mathbf{J}_{O}(\Theta)\dot{\Theta}, \end{cases} \tag{8}$$

where $\mathbf{S}(\cdot)$ is the skew-symmetric matrix.

For the sake of simplicity, the kinematic model using a matrix form is described as

$$\begin{bmatrix} \dot{\mathbf{p}} \\ \omega \\ {}^{I}\dot{\mathbf{p}}_{i} \\ {}^{I}\omega_{i} \end{bmatrix} = \begin{bmatrix} \mathbf{I}_{3\times3} & \mathbf{0}_{3\times3} & \mathbf{0}_{3\times2} \\ \mathbf{0}_{3\times3} & \mathbf{T} & \mathbf{0}_{3\times2} \\ \mathbf{I}_{3\times3} & -\mathbf{S}\left({}^{I}\mathbf{R}_{B}{}^{B}\mathbf{p}_{i}\right)\mathbf{T} & {}^{I}\mathbf{R}_{B}\mathbf{J}_{P}(\Theta) \\ \mathbf{0}_{3\times3} & \mathbf{T} & {}^{I}\mathbf{R}_{B}\mathbf{J}_{O}(\Theta) \end{bmatrix} \mathbf{q} = \begin{bmatrix} \mathbf{A}_{1} \\ \mathbf{A}_{2} \\ \mathbf{A}_{3} \\ \mathbf{A}_{4} \end{bmatrix} \dot{\mathbf{q}}. \tag{9}$$

2.2. Dynamics. To describe the relationship between inputs and motion of the aerial robot, the dynamic model derived by the Lagrange equation is given by [23]

$$\frac{d}{dt}\left(\frac{\partial L}{\partial \dot{\mathbf{q}}}\right)^{T} - \left(\frac{\partial L}{\partial \mathbf{q}}\right)^{T} = \tau + \tau_{D}, \tag{10}$$

$$L = K - U, \tag{11}$$

where τ is the generalized torque associated with the generalized coordinate. τ_{D} indicates external disturbance applied to the system. L is the Lagrangian expressed as the difference between kinetic energy K and potential energy U.

The kinematic energy is governed by the sum of the motion of the hexarotor and manipulator, which is written as

$$K = K_{B} + \sum_{i=1}^{2} K_{i}, \tag{12}$$

where

$$K_{B} = \frac{1}{2}m_{B}\dot{\mathbf{p}}^{T}\dot{\mathbf{p}} + \frac{1}{2}\dot{\Omega}^{T}\mathbf{T}^{TI}\mathbf{R}_{B}\mathbf{I}_{B}{}^{I}\mathbf{R}_{i}^{T}\mathbf{T}\dot{\Omega}, \tag{13}$$

$$K_{i} = \frac{1}{2}m_{i}{}^{I}\dot{\mathbf{p}}_{i}^{T}{}^{I}\dot{\mathbf{p}}_{i} + \frac{1}{2}{}^{I}\omega_{i}^{T}{}^{I}\mathbf{R}_{i}\mathbf{I}_{i}{}^{I}\mathbf{R}_{i}^{T}{}^{I}\omega_{i}, \tag{14}$$

where m and $\mathbf{I}$ are mass and inertia moment, respectively.

As done for kinematic energy, the potential energy stored in the aerial robot is given by

$$U = m_{B}g\mathbf{e}_{3}^{T}\mathbf{p} + \sum_{i=1}^{2} m_{i}g\mathbf{e}_{3}^{T}\left(\mathbf{p} + {}^{I}\mathbf{R}_{B}{}^{B}\mathbf{p}_{i}\right), \tag{15}$$

where $\mathbf{e}_{3} = [0, 0, 1]^{T}$ and g is the gravity.

Introduce equations (11)-(15) into equation (10), yielding

$$\mathbf{M}(\mathbf{q})\ddot{\mathbf{q}} + \mathbf{C}(\mathbf{q}, \dot{\mathbf{q}})\dot{\mathbf{q}} + \mathbf{G}(\mathbf{q}) = \tau + \tau_{D}, \tag{16}$$

where the inertia matrix $\mathbf{M}(\mathbf{q})$, the Coriolis matrix $\mathbf{C}(\mathbf{q}, \dot{\mathbf{q}})$, and the gravity matrix $\mathbf{G}(\mathbf{q})$ are calculated as

$$\begin{aligned}\mathbf{M}(\mathbf{q}) = {} & \mathbf{A}_1^T m_B \mathbf{A}_1 + \mathbf{A}_2^{TI} \mathbf{R}_B \mathbf{I}_B{}^I \mathbf{R}_B^T \mathbf{A}_2 \\ & + \sum_{i=1}^{2} \left\{ \mathbf{A}_3^T m_i \mathbf{A}_3 + \mathbf{A}_4^{TI} \mathbf{R}_i \mathbf{I}_i{}^I \mathbf{R}_i^T \mathbf{A}_4 \right\},\end{aligned} \tag{17}$$

$$\mathbf{C}(\mathbf{q}, \dot{\mathbf{q}})\dot{\mathbf{q}} = \dot{\mathbf{M}}(\mathbf{q})\dot{\mathbf{q}} - \frac{1}{2}\left(\frac{\partial}{\partial \mathbf{q}}\left(\dot{\mathbf{q}}^T \mathbf{M}(\mathbf{q})\dot{\mathbf{q}}\right)\right)^T, \tag{18}$$

$$\mathbf{G}(\mathbf{q}) = \frac{\partial U}{\partial \mathbf{q}}. \tag{19}$$

In the dynamic model, the generalized torque contains two components. Regarding the joint torque, each joint is driven by an actuator (direct drive or gear drive). Indeed, the torque could be calculated through the current and torque constant [24]. With respect to the hexarotor, the forces and torques actuated by six propellers are expressed in the following form:

$$\begin{cases} F = \sum_{i=1}^{6} f_i, \\ \tau_\phi = \left[(f_1 + f_3 - f_4 - f_6) \sin\dfrac{\pi}{6} + f_2 - f_5 \right] \cdot l, \\ \tau_\theta = (f_3 + f_4 - f_1 - f_6) \sin\dfrac{\pi}{3} \cdot l, \\ \tau_\psi = \tau_{m1} + \tau_{m3} + \tau_{m5} - \tau_{m2} - \tau_{m4} - \tau_{m6}, \end{cases} \tag{20}$$

where $f_i (i = 1, \cdots, 6)$ and $\tau_{mi} (i = 1, \cdots, 6)$ are thrust and moment produced by the motors, respectively. l is the lever length from the centre of a propeller to the centre of the vehicle body.

Since the hexarotor flies in a trimmed condition, its dynamic model can be reduced into a simplified form [25, 26]. Therefore, the nominal relation of the inputs to the aerial robot and generalized torque is rewritten as:

$$\tau = \begin{bmatrix} \mathbf{N}_{3\times1} & \mathbf{0}_{3\times3} & \mathbf{0}_{3\times2} \\ \mathbf{0}_{3\times1} & \mathbf{T}^{TI}\mathbf{R}_B & \mathbf{0}_{3\times2} \\ \mathbf{0}_{2\times1} & \mathbf{0}_{2\times3} & \mathbf{I}_{2\times2} \end{bmatrix} \begin{bmatrix} F \\ \tau_\phi \\ \tau_\theta \\ \tau_\psi \\ \tau_{\varepsilon_1} \\ \tau_{\varepsilon_2} \end{bmatrix}, \tag{21}$$

where

$$\mathbf{N} = [\theta \cos\psi + \phi \sin\psi, \theta \sin\psi - \phi \cos\psi, 1]^T. \tag{22}$$

3. Robust Control Strategy

From the relation of the aerial robot displayed in equations (10)-(21), the input and output present a second-order derivative relation, which is shown in Figure 2. In other words, the dynamic model of the aerial robot can be regarded as eight second-order subsystems. In this section, the design of a LADRC for each subsystem will be introduced.

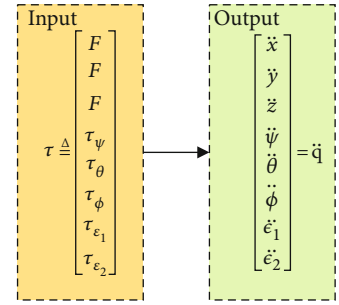

Figure 2: Inputs and outputs of the aerial robot.

Consider a second-order plant:

$$\begin{cases} \ddot{x}_s = f_s(x_s, \dot{x}_s, w_s, t) + bu, \\ y_s = x_s, \end{cases} \tag{23}$$

where x_s, u, and y_s are the state variable, system input, and system output, respectively.

Suppose b_0 is the approximate value of b, system (23) is rewritten as

$$\begin{cases} \ddot{x}_s = f_s + (b - b_0)u + b_0 u = f + b_0 u, \\ y_s = x_s. \end{cases} \tag{24}$$

Remark 1. The lumped disturbance f is another form of the term $f_s(x_s, \dot{x}_s, w_s, t)$, which contains parametric uncertainties, external disturbance, and complex nonlinear dynamics.

Assumption 1. Assume that the lumped disturbance f is differentiable and bounded. It indicates $\|f\| < \infty$ and $\|\dot{f}\| < \infty$, and their bounds are defined as $\sup_{t>0}\|f\| = f_b$ and $\sup_{t>0}\|\dot{f}\| = h_b$, respectively.

Using a state-space form to describe the system (24) yields

$$\begin{cases} \dot{\mathbf{x}} = \mathbf{A}\mathbf{x} + \mathbf{B}\mathbf{u} + \mathbf{E}\mathbf{h}, \\ \mathbf{y} = \mathbf{C}\mathbf{x}, \end{cases} \tag{25}$$

where

$$\mathbf{A} = \begin{bmatrix} 0 & 1 & 0 \\ 0 & 0 & 1 \\ 0 & 0 & 0 \end{bmatrix}, \tag{26}$$

$$\mathbf{B} = \begin{bmatrix} 0 \\ b_0 \\ 0 \end{bmatrix}, \tag{27}$$

$$\mathbf{C} = \begin{bmatrix} 1 \\ 0 \\ 0 \end{bmatrix}^T, \tag{28}$$

$$\mathbf{E} = \begin{bmatrix} 0 \\ 0 \\ 1 \end{bmatrix}. \tag{29}$$

Now f can be estimated using an additional state variable. The so-called LESO of system (25) is constructed as

$$\begin{cases} \dot{\mathbf{z}} = \mathbf{A}\mathbf{z} + \mathbf{B}\mathbf{u} + \mathbf{L}(\mathbf{y} - \hat{\mathbf{y}}), \\ \hat{\mathbf{y}} = \mathbf{C}\mathbf{z}, \end{cases} \tag{30}$$

and $\mathbf{L}$ is the observer gain, which is calculated by a pole placement method [19]:

$$\mathbf{L} = \begin{bmatrix} l_1 \\ l_2 \\ l_3 \end{bmatrix} = \begin{bmatrix} 3\omega_o \\ 3\omega_o{}^2 \\ \omega_o{}^3 \end{bmatrix}, \tag{31}$$

where $\omega_o > 0$ is the observer bandwidth. As a result, z_i tracks $x_i (i = 1, 2)$ and z_3 estimates f. By eliminating the effect of f, the LADRC actively compensates for lumped disturbances in real-time.

The control law is designed as

$$u = \frac{u_0 - z_3}{b_0}. \tag{32}$$

Then, the plant in system (23) is converted into a unit double integrator, which is easily stabilized with a PD controller:

$$\ddot{y} = f - z_3 + u_0 \approx u_0 = \lambda_1 (r_e - z_1) - \lambda_2 z_2, \tag{33}$$

where r_e is the referenced signal. The closed-loop transfer function pure second order without zero is given by

$$G_2 = \frac{\lambda_1}{s^2 + \lambda_2 s + \lambda_1}. \tag{34}$$

Similarly, the λ_1 and λ_2 are calculated by a pole placement method, namely, $\lambda_1 = \omega_c{}^2$ and $\lambda_2 = 2\omega_c$, respectively. ω_c is the control bandwidth.

The aerial robot system is constructed from the attitude loop, position loop to manipulator loop according to the time-scale separation principle. Each loop is controlled by the LADRC, as shown in Figure 3.

4. Controller Analysis

4.1. Stability Analysis. In this section, the stability analysis of LADRC will be given as follows.

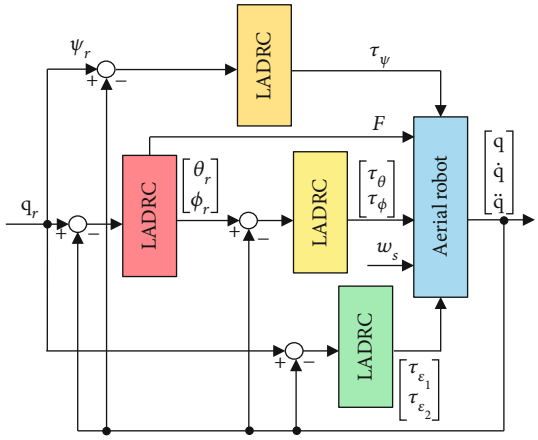

Figure 3: Control structure of the aerial robot.

Prove the tracking error is bounded. Subtracting equation (30) from (25) yields

$$\dot{\mathbf{e}} = \mathbf{A}_e \mathbf{e} + \mathbf{E}\mathbf{h}, \tag{35}$$

where $\mathbf{e}$ is the so-called observer error caused by the adoption of LESO. $\mathbf{A}_e$ is written as

$$\mathbf{A}_e = \mathbf{A} - \mathbf{L}\mathbf{C} = \begin{bmatrix} -3\omega_o & 1 & 0 \\ -3\omega_o{}^2 & 0 & 1 \\ \omega_o{}^3 & 0 & 0 \end{bmatrix}. \tag{36}$$

Obviously, the LESO is bounded-input and bounded-output (BIBO) stable if the eigenvalues of the characteristic polynomial of $\mathbf{A}_e$ are all in the left half plane. Besides, $\mathbf{e}$ is bounded for the arbitrary bound $\mathbf{h}$.

Lemma 1. *Suppose the LESO and the control law in equation (33) are stable, the design of LADRC yields a BIBO stable closed-loop system.*

Substituting equation (33) to (32) yields

$$u = \frac{1}{b_0} \begin{bmatrix} -\lambda_1 & -\lambda_2 & -1 \end{bmatrix} \begin{bmatrix} z_1 - r_e \\ z_2 \\ z_3 \end{bmatrix} = \mathbf{Q}\mathbf{z} - \frac{1}{b_0} \begin{bmatrix} r_e \\ 0 \\ 0 \end{bmatrix} = \mathbf{Q}\mathbf{z} - \mathbf{G}, \tag{37}$$

where

$$\mathbf{Q} = \frac{1}{b_0} \begin{bmatrix} -\lambda_1 & -\lambda_2 & -1 \end{bmatrix}. \tag{38}$$

Equations (25) and (30) are rearranged as

$$\begin{bmatrix} \dot{\mathbf{x}} \\ \dot{\mathbf{z}} \end{bmatrix} = \begin{bmatrix} \mathbf{A} & \mathbf{BQ} \\ \mathbf{LC} & \mathbf{A} - \mathbf{LC} + \mathbf{BQ} \end{bmatrix} \begin{bmatrix} \mathbf{x} \\ \mathbf{z} \end{bmatrix} + \begin{bmatrix} -\mathbf{B} & \mathbf{E} \\ -\mathbf{B} & \mathbf{0} \end{bmatrix} \begin{bmatrix} \mathbf{G} \\ \mathbf{h} \end{bmatrix}. \tag{39}$$

Then, one gets

$$\begin{aligned} &\operatorname{eig}\left(\begin{bmatrix} \mathbf{A} & \mathbf{BQ} \\ \mathbf{LC} & \mathbf{A} - \mathbf{LC} + \mathbf{BQ} \end{bmatrix}\right) \\ &\quad = \operatorname{eig}\left(\begin{bmatrix} \mathbf{A} + \mathbf{BQ} & \mathbf{BQ} \\ 0 & \mathbf{A} - \mathbf{LC} \end{bmatrix}\right) \\ &\quad = \operatorname{eig}(\mathbf{A} + \mathbf{BQ}) \cup \operatorname{eig}(\mathbf{A} - \mathbf{LC}) \\ &\quad = \operatorname{root}\left(s^2 + \lambda_1 s + \lambda_2\right) \cup \operatorname{root}\left(s^2 + 3\omega_o s^2 + 3\omega_o s + {\omega_o}^3\right). \end{aligned} \tag{40}$$

Similarly, the control system is BIBO stable if the eigenvalues of equation (40) are in the left half plane. Because the referenced signal r_e is always bounded, the only nontrivial condition is that f is differentiable.

4.2. Parameter Tuning. In the robust controller, the parameters ω_o, ω_c, and b_0 together affect the control performance. To obtain the appropriate control parameters, parameter tuning is crucial. In this regard, the artificial intelligence algorithm may be a useful method. Several reports about this application have been found in Refs. [27, 28]. In this paper, a famous artificial bee colony (ABC) algorithm is introduced to optimize the parameters in LADRC. Based on the ABC algorithm, a cost function capturing the performance of the controller is minimized over a sequence of step inputs. An improved integral of time multiplied by absolute error (IITAE) criterion is selected as the cost function:

$$F_c = c_1 \int_0^\infty t|e(t)|dt + c_2 \int_0^\infty (u(t))^2 dt + c_3 t_s + c_4 o_s, \tag{41}$$

where F_c denotes the cost function. $|e(t)|$ and $u(t)$ are the tracking error and control signal in the time domain, respectively. t_s is the settling time, o_s is the overshoot, and c_1~c_4 are the weight coefficients.

Before the experiment, parameter tuning is conducted in the MATLAB environment with a fixed sampling time of 16 s, which is similar to the one reported in Ref. [29]. The simulation with 100 runs is repeated five times so as to obtain the best result. The result of the parameter tuning is shown in Figures 4–6. With the proposed method, the optimal control parameters can be found in a finite time.

Taking the attitude loop as an example, the response to step inputs is plotted in Figure 7. In the loop, the mean of 0 and covariance of 0.01 stochastic noises are added in the input ports. In spite of the disturbances, all the responses of the attitude angles can track the referenced signal with approximately 5 s. The simulation demonstrates the efficiency of the proposed controller in attitude tacking with high accuracy and fast convergence rate.

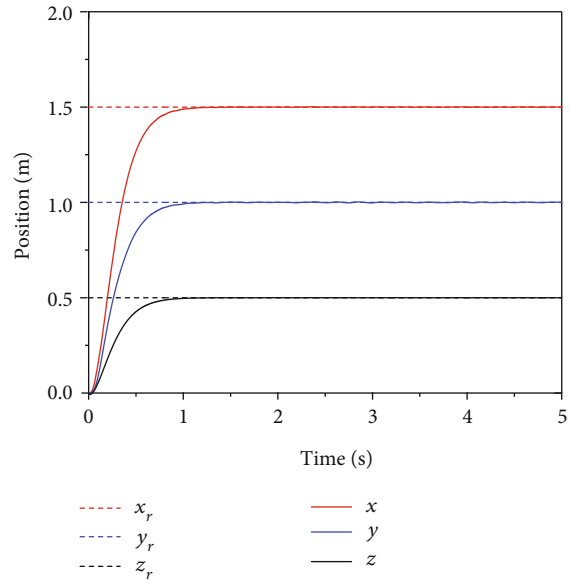

Figure 4: Response of the position loop.

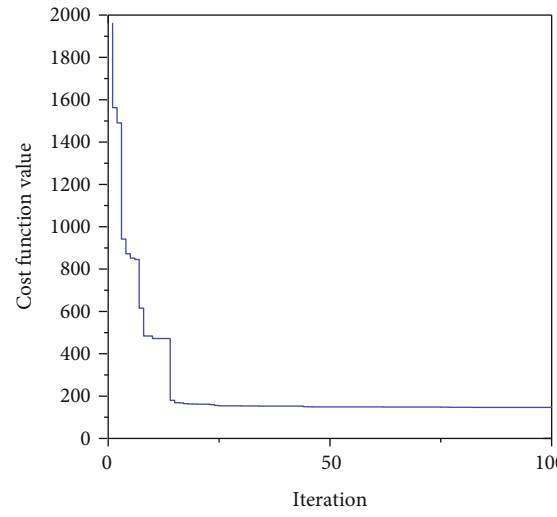

Figure 5: Evolving curve of the ABC algorithm.

Another important criterion to evaluate the suitability and robustness of the LADRC is to analyse the control performance by comparing with other controllers, such as PID. Similarly, the control parameter adjustment followed standard methods for tuning the PID [30]. The result from Figure 8 indicates that the roll angle based on LADRC has stronger robustness with respect to disturbances than the one based on PID. Note that the attitude loop is always running at a higher frequency than the position loop to guarantee that the Euler angles are close to zero.

In addition, the effects of wind and aerodynamics such as blade flapping as well as aerodynamic drag are neglected in hexarotor dynamics in equation (20). The detailed discussions about these effects on multirotors can be found in Ref. [31]. The role of this simulation is to acquire a set of

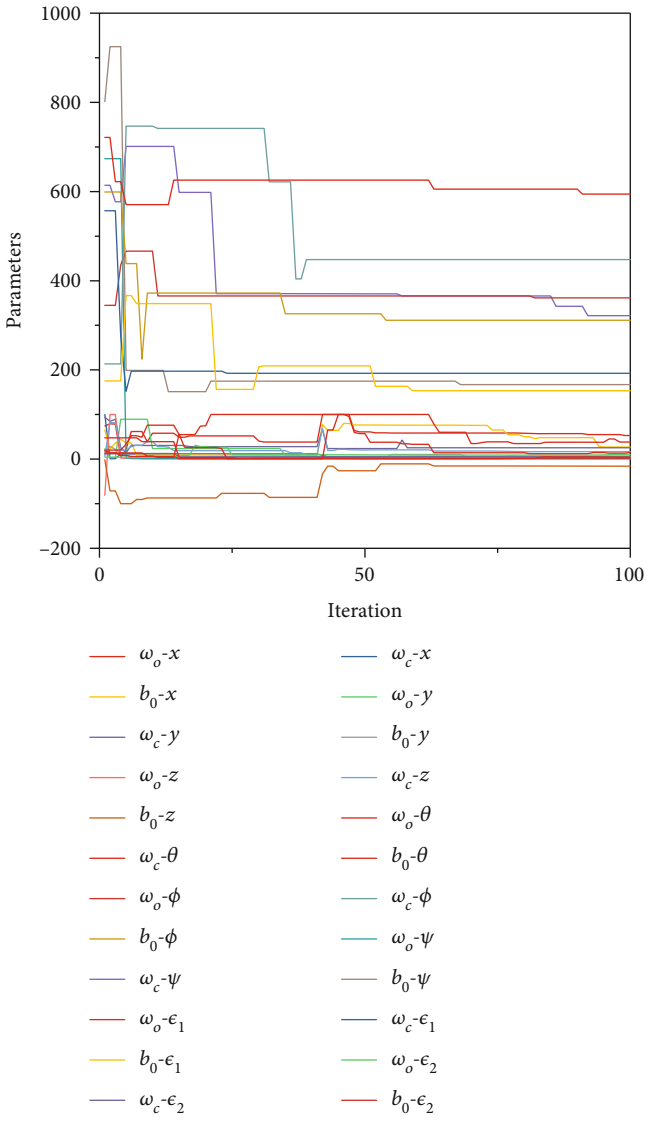

Figure 6: Dynamic process of parameter tuning.

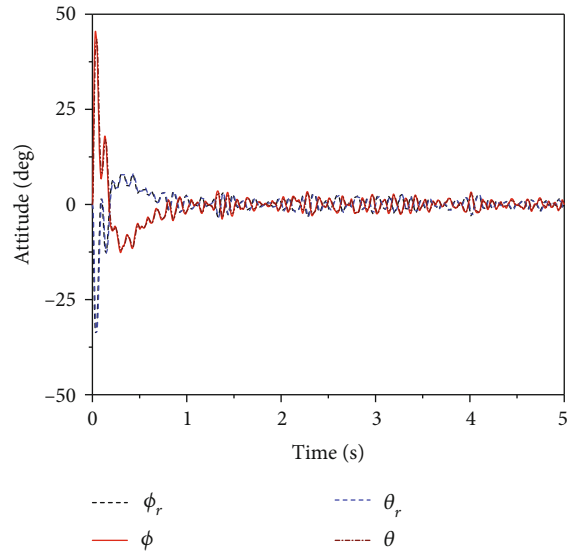

Figure 7: Response of the roll angle and pitch angle.

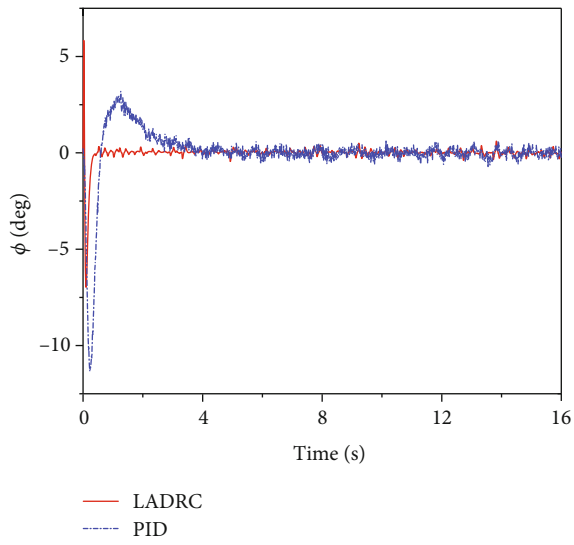

Figure 8: Response of the roll angle.

applicable control parameters for the following experiments. Subjected to the poor experimental condition, the wind and aerodynamics could not be measured. Hence, these factors as well as modelling uncertainties are substituted by stochastic noise.

5. Experimental Validation

5.1. Experiment Setup. This section presents real-time experimental results obtained when applying the proposed robust controller for the aerial robot. Figure 9 shows the experimental platform designed to investigate the maneuverability of the aerial robot. The platform consists of a hexarotor equipped with a 2-DOF manipulator, a Futaba remote control unit, a ground station, a Pixhawk controller, a global position system (GPS), and a couple of XBee wireless data links. The ground station sends a series of commands to the aerial robot via the XBee at a frequency of 50 Hz. Meanwhile, it collects and saves the experimental data in real-time. If some faults occur during the automatic control, the operator will manually manipulate the aerial robot by the Futaba.

Tables 1 and 2 summarized the aerial robot parameters, including mass, inertia moment, and standard Denavit-Hartenberg (DH) parameters. The inertia moments are measured by a two-line method, which is referred to in Ref. [32].

In the experiment, the aerial robot is driven to perform three tasks. More specifically, the tasks consist of taking off, grabbing a 0.3 kg water bottle and dropping it in the designated area during flight, and landing. The planar graph of the experimental environment is depicted in Figure 10.

5.2. Experiment Results. With the flight path planned in the ground station, the flight tasks are emulated in MATLAB environment. Then, the control scheme, including the adjusted control parameters, is transformed to C-codes

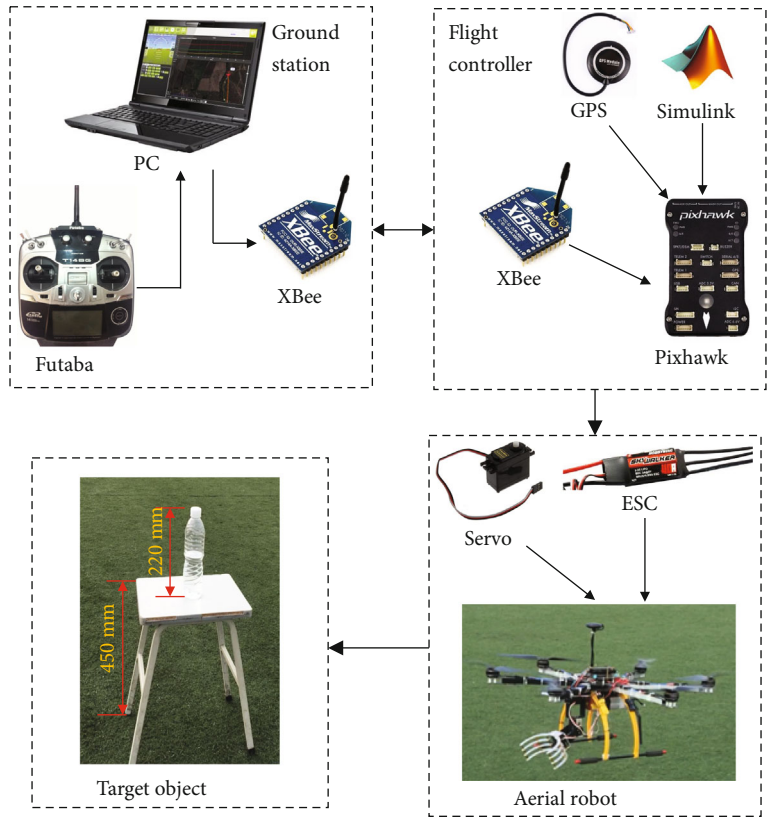

Figure 9: Structure of the equipment platform.

Table 1: Aerial robot parameters.

Parameter	Hexarotor	Link 1	Link 2
m (kg)	3.64	0.164	0.409
I_{xx} (kg·m^2)	7.2×10^{-2}	1.9×10^{-4}	2.2×10^{-4}
I_{yy} (kg·m^2)	6.9×10^{-2}	2.6×10^{-4}	1.8×10^{-4}
I_{zz} (kg·m^2)	1.1×10^{-2}	3.7×10^{-4}	1.5×10^{-4}

Table 2: Standard DH parameters of the manipulator.

Parameter	Value	
Link i	1	2
Link twist (deg)	90	0
Link length (mm)	50	103
Link offset (mm)	0	0
Joint angle (deg)	-60~10	-90~90

through the Pixhawk pilot support package (PSP) [33]. We perform the flight experiments sixteen times, and the result of the trials is given in Figure 11. The results show that finishing all the tasks has a high degree of difficulty with a barely 31.25 percent success rate. The main reason is that it is difficult to stabilize the attitude and position of the aerial robot during grabbing of the bottle.

During the experiment, the flight altitude of the aerial robot is set at 1 m to reduce the effect of air as much as possible. The results are summarized in Figures 12–16. First of all, in Figure 11, it is clear that all the tasks have been accomplished. The snapshots in Figure 12(b)–12(d) also show the process of the aerial robot manipulating the bottle from the stool. At that moment, the aerial robot provides a stable attitude and position through the LADRC controller.

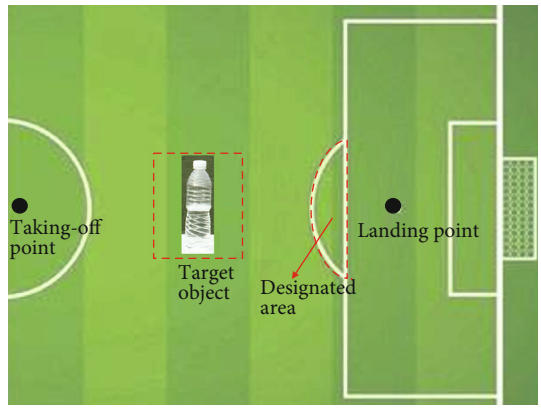

Figure 10: Sketch of experiment environment.

Figure 13 depicts the position tracking curves in three axes using the GPS sensor while flying missions. From the results, we find that the control performance degrades significantly when the manipulator moves, especially in the process of grabbing the bottle or dropping it. That may be attributed to the dynamical coupling between the hexarotor and manipulator.

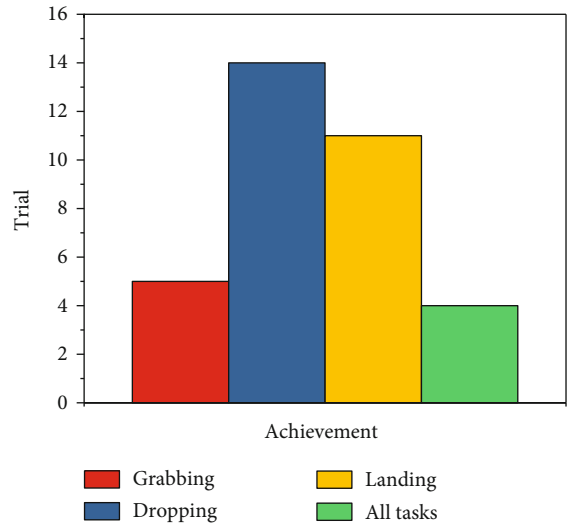

Figure 11: Results of the trials.

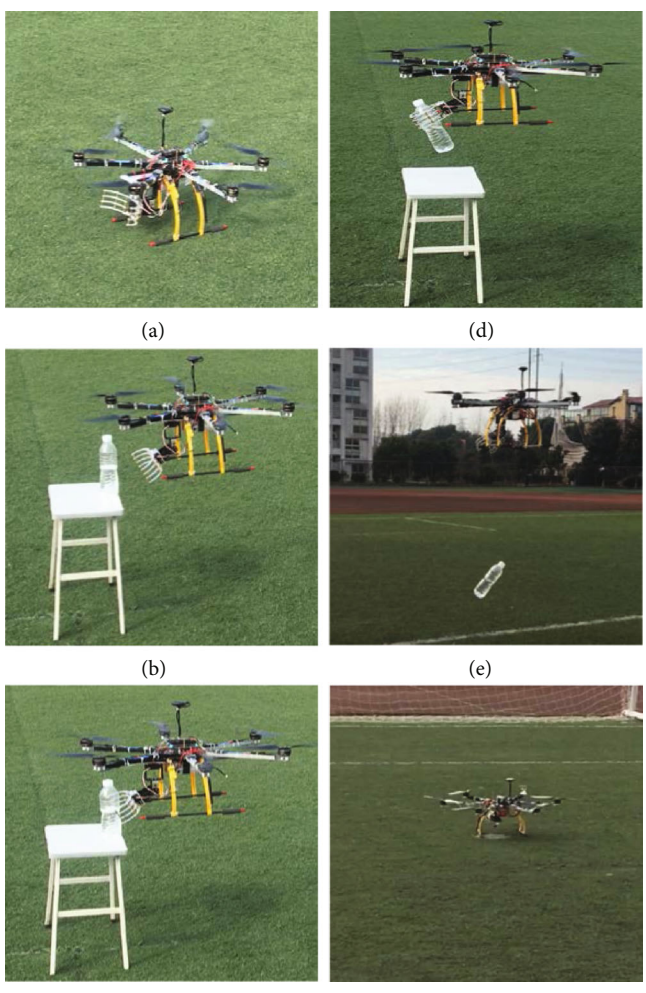

Figure 12: Snapshots of the objective operation.

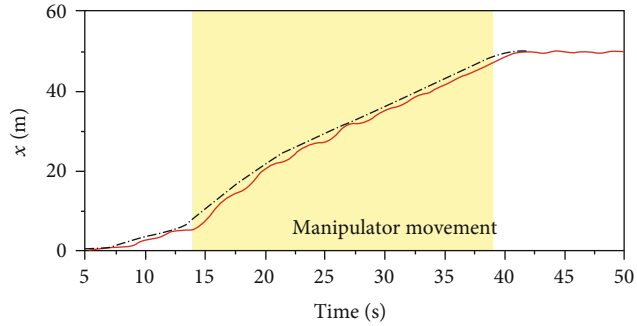

(a) x-position

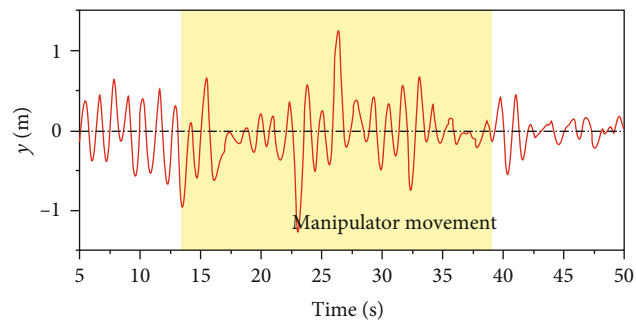

(b) y-position

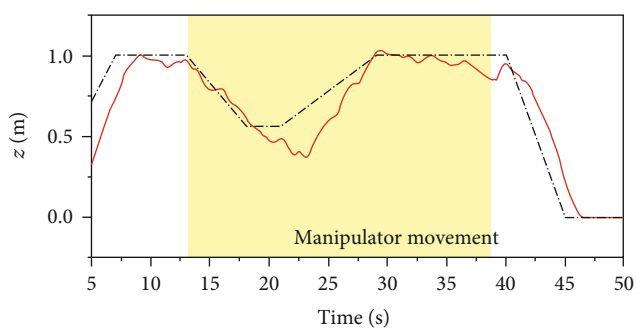

(c) z-position

Figure 13: Position trajectories in time history.

To further evaluate the control performance of the position loop, root-mean-square-error (RMSE) and maximum-error (ME) values are calculated between the referenced and actual positions, which are given in Table 3. As mentioned in Section 4, the slow position responses cause errors to accumulate as the goal reference is reached. Nevertheless, it can be observed that the position tracking is achieved with acceptable tracking errors in the presence of external disturbances and manipulator movement.

In addition, the other state variables of the aerial robot are displayed in Figures 14–16. Based on the proposed control scheme, these system states have slight chattering due to measurement noise. There are some surge oscillations

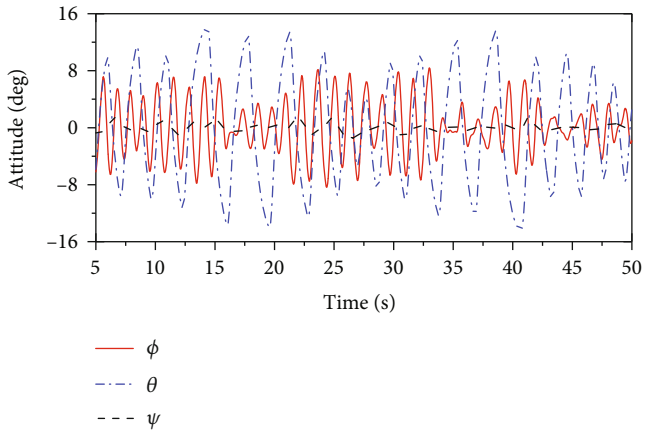

Figure 14: Attitude trajectories in time history.

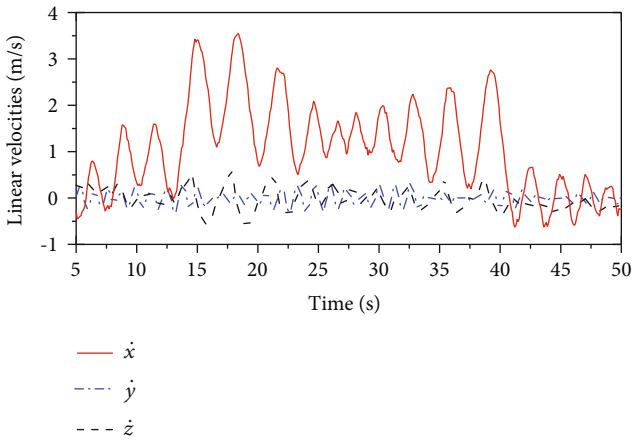

Figure 15: Linear velocities in time history.

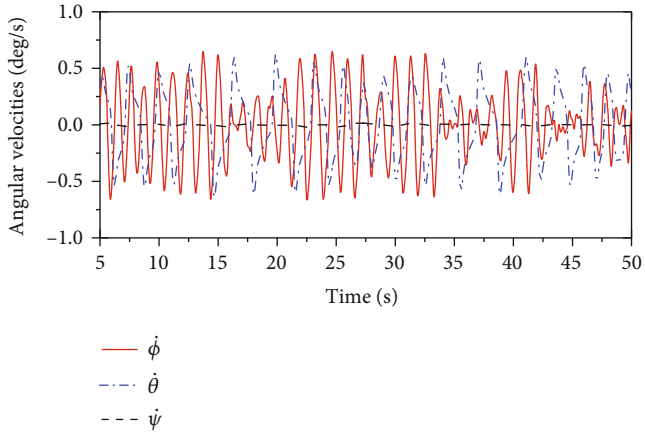

Figure 16: Angular velocities in time history.

while the end-effector grabs or drops the bottle in the time intervals ([20, 25] and [35, 37], respectively). As a result, the change of load can affect the control performance of the position and attitude of the aerial robot. Despite that, all the state variables are stabilized within an acceptable limit.

Table 3: RMSE and ME of position loop.

Index	x (m)	y (m)	z (m)
RMSE	10.155	1.575	2.471
ME	3.778	0.243	0.277

Table 4: Variation of two joint angles.

Time (s)	ε_1 (deg)	ε_2 (deg)
5	0	-30
13	-60	0
21	-60	0
27	0	-30
50	0	-30

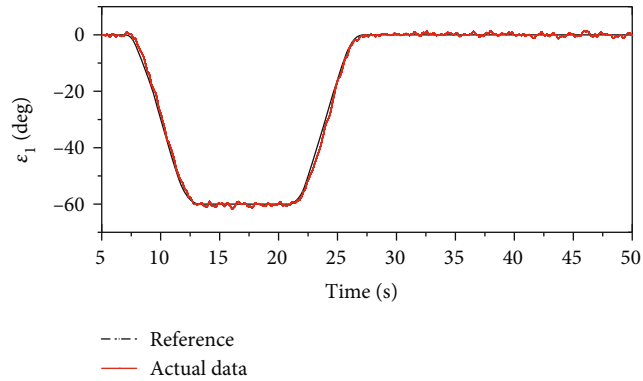

(a) Torque of joint 1

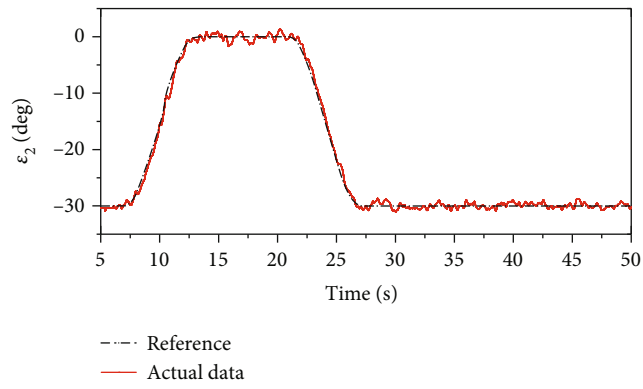

(b) Torque of joint 2

Figure 17: Joints of the manipulator in time history.

It confirms the robustness of the proposed control technique with respect to the abrupt disturbances.

During the experiment, the variation of the two joint angles is displayed in Table 4. The trajectories in joint space are planned by the third-order polynomial. Polynomial function is simple to compute and can easily provide smooth waypoints. The outputs of the manipulator are given in Figure 17, where the raw data can be observed by encoders. From the results, the actual responses of the joints match the referenced trajectories well in spite of lumped disturbances

and dynamic coupling from the hexarotor. It indicates that the developed dynamic model can reflect the dynamic behaviour of the aerial robot, and the proposed controller can obtain a satisfying operating performance. However, the force applied to each joint could not be measured due to the lack of force sensors. A satisfactory force control performance could be expected in practice if there are high-cost sensors. This issue will be investigated in our future work.

6. Conclusion

We have presented modelling and control techniques to perform an aerial robot using an unmanned hexarotor and multiple-degree manipulator arms. The system model of the aerial robot is established by the Euler-Lagrange method, including the kinematics and dynamics. Based on the model, a robust controller using the LADRC method is presented to manipulate the system. Moreover, the suitable control performance can be obtained by the ABC algorithm. Through some numerical simulation cases, it is demonstrated that the proposed controller has good robustness against parametric uncertainties and external disturbances, compared to the PID method. With the proposed controller, the attitude loop, position loop, and manipulator loop are stabilized while the aerial robot performs the aerial tasks. The successful experimental results indicate that the proposed control method can be a practical solution for aerial manipulation.

Data Availability

The parameters of the aerial robot we used have been shown in the paper. The data of the simulations and experiments can be provided if necessary.

Conflicts of Interest

The authors declare that they have no conflicts of interest.

Authors' Contributions

Li Ding, Zhenqi Gao, Ming Huang, and Hongtao Wu contributed equally to this work.

Acknowledgments

Helpful discussions with Professor Yu Yao from Nanjing University of Aeronautics and Astronautics on his guidance in the control theory of aerial robots are gratefully acknowledged. This work was partially supported by the Foundation Research Project of Jiangsu Province (the Natural Science Fund No. BK20170315), Changzhou Sci&Tech Program of China (Grant No. CJ20179017).

References

[1] M. Orsag, C. Korpela, S. Bogdan, and P. Oh, "Dexterous aerial robots—mobile manipulation using unmanned aerial systems," *IEEE Transactions on Robotics*, vol. 33, no. 6, pp. 1453–1466, 2017.

[2] A. E. Jimenez-Cano, G. Heredia, M. Bejar, K. Kondak, and A. Ollero, "Modelling and control of an aerial manipulator consisting of an autonomous helicopter equipped with a multi-link robotic arm," *Proceedings of the Institution of Mechanical Engineers, Part G: Journal of Aerospace Engineering*, vol. 230, no. 10, pp. 1860–1870, 2016.

[3] E. Khanmirza, K. Daneshjou, and A. K. Ravandi, "Underactuated flexible aerial manipulators: a new framework for optimal trajectory planning under constraints induced by complex dynamics," *Journal of Intelligent & Robotic Systems*, vol. 92, no. 3-4, pp. 599–613, 2018.

[4] T. W. Danko and P. Y. Oh, "Design and control of a hyper-redundant manipulator for mobile manipulating unmanned aerial vehicles," *Journal of Intelligent & Robotic Systems*, vol. 73, no. 1-4, pp. 709–723, 2014.

[5] K. Baizid, G. Giglio, F. Pierri et al., "Behavioral control of unmanned aerial vehicle manipulator systems," *Autonomous Robots*, vol. 41, no. 5, pp. 1203–1220, 2017.

[6] S. Kim, H. Seo, J. Shin, and H. J. Kim, "Cooperative aerial manipulation using multirotors with multi-dof robotic arms," *IEEE/ASME Transactions on Mechatronics*, vol. 23, no. 2, pp. 702–713, 2018.

[7] M. Orsag, C. M. Korpela, S. Bogdan, and P. Y. Oh, "Hybrid adaptive control for aerial manipulation," *Journal of Intelligent & Robotic Systems*, vol. 73, no. 1-4, pp. 693–707, 2014.

[8] P. E. Pounds and A. M. Dollar, "Aerial grasping from a helicopter UAV platform," in *Experimental Robotics*, pp. 269–283, Springer, Berlin, Heidelberg, 2014.

[9] X. Ding and S. Yu, "A multi-propeller and multi-function aero-robot and its motion planning of leg-wall-climbing," *Acta Aeronautica Et Astronautica Sinica*, vol. 10, 2010.

[10] H. Abaunza, P. Castillo, A. Victorino, and R. Lozano, "Dual quaternion modeling and control of a quad-rotor aerial manipulator," *Journal of Intelligent & Robotic Systems*, vol. 88, no. 2-4, pp. 267–283, 2017.

[11] G. Mohamed, A. A. Sofiane, and L. Nicolas, "Adaptive super twisting extended state observer based sliding mode control for diesel engine air path subject to matched and unmatched disturbance," *Mathematics and Computers in Simulation*, vol. 151, pp. 111–130, 2018.

[12] K. Ryu and J. Back, "An output feedback coordinated tracking controller for high-order linear systems," *International Journal of Control, Automation and Systems*, vol. 13, no. 6, pp. 1360–1368, 2015.

[13] G. Rigatos, P. Siano, and N. Zervos, "Sensorless control of distributed power generators with the derivative-free nonlinear Kalman filter," *IEEE Transactions on Industrial Electronics*, vol. 61, no. 11, pp. 6369–6382, 2014.

[14] F. Rinaldi, S. Chiesa, and F. Quagliotti, "Linear quadratic control for quadrotors UAVs dynamics and formation flight," *Journal of Intelligent & Robotic Systems*, vol. 70, no. 1-4, pp. 203–220, 2013.

[15] T. Baca, G. Loianno, and M. Saska, "Embedded model predictive control of unmanned micro aerial vehicles," in *2016 21st international conference on methods and models in automation and robotics (MMAR)*, pp. 992–997, Miedzyzdroje, Poland, 2016.

[16] J. Gadewadikar, F. L. Lewis, K. Subbarao, K. Peng, and B. M. Chen, "H-infinity static output-feedback control for rotorcraft," *Journal of Intelligent and Robotic Systems*, vol. 54, no. 4, pp. 629–646, 2009.

[17] M. Orsag, C. Korpela, and P. Oh, "Modeling and control of MM-UAV: mobile manipulating unmanned aerial vehicle," *Journal of Intelligent & Robotic Systems*, vol. 69, no. 1-4, pp. 227–240, 2013.

[18] S. Kim, H. Seo, S. Choi, and H. J. Kim, "Vision-guided aerial manipulation using a multirotor with a robotic arm," *IEEE/ASME Transactions on Mechatronics*, vol. 21, no. 4, pp. 1912–1923, 2016.

[19] Z. Gao, "Scaling and bandwidth-parameterization based controller tuning," in *Proceedings of the 2003 American Control Conference*, Denver, CO, USA, USA, 2003.

[20] J. Zhang, J. Feng, Y. Zhou, F. Fang, and H. Yue, "Linear active disturbance rejection control of waste heat recovery systems with organic Rankine cycles," *Energies*, vol. 5, no. 12, pp. 5111–5125, 2012.

[21] Y. Liu, J. Liu, and S. Zhou, "Linear active disturbance rejection control for pressurized water reactor power," *Annals of Nuclear Energy*, vol. 111, pp. 22–30, 2018.

[22] P. Corke, *Robotics, Vision and Control: Fundamental Algorithms in MATLAB® Second, Completely Revised*, vol. 118, Springer, 2017.

[23] Y. Sun, G. Ma, M. Liu, C. Li, and J. Liang, "Distributed finite-time coordinated control for multi-robot systems," *Transactions of the Institute of Measurement and Control*, vol. 40, no. 9, pp. 2912–2927, 2018.

[24] L. Ding, X. Li, Q. Li, and Y. Chao, "Nonlinear friction and dynamical identification for a robot manipulator with improved cuckoo search algorithm," *Journal of Robotics*, vol. 2018, Article ID 8219123, 2018.

[25] W. Dong, G.-Y. Gu, X. Zhu, and H. Ding, "High-performance trajectory tracking control of a quadrotor with disturbance observer," *Sensors and Actuators A: Physical*, vol. 211, pp. 67–77, 2014.

[26] L. Ding, H. Wu, and X. Li, "Trakectory tracking congrol for an unmanned hexrotor with lumped distrubances," *Chinese Journal of Engineering*, vol. 40, no. 5, 628 pages, 2018.

[27] O. A. Sahed, K. Kara, A. Benyoucef, and M. L. Hadjili, "An efficient artificial bee colony algorithm with application to nonlinear predictive control," *International Journal of General Systems*, vol. 45, no. 4, pp. 393–417, 2016.

[28] B. Afşar, D. Aydin, A. Uğur, and S. Korukoğlu, "Self-adaptive and adaptive parameter control in improved artificial bee colony algorithm," *Informatica*, vol. 28, no. 3, pp. 415–438, 2017.

[29] L. Ding, R. Ma, H. Wu, C. Feng, and Q. Li, "Yaw control of an unmanned aerial vehicle helicopter using linear active disturbance rejection control," *Proceedings of the Institution of Mechanical Engineers, Part I: Journal of Systems and Control Engineering*, vol. 231, no. 6, pp. 427–435, 2017.

[30] Y. Nishikawa, N. Sannomiya, T. Ohta, and H. Tanaka, "A method for auto-tuning of PID control parameters," *Automatica*, vol. 20, no. 3, pp. 321–332, 1984.

[31] Y. Guo, B. Jiang, and Y. Zhang, "A novel robust attitude control for quadrotor aircraft subject to actuator faults and wind gusts," *IEEE/CAA Journal of Automatica Sinica*, vol. 5, no. 1, pp. 292–300, 2018.

[32] Y. Liu, C. Chen, H. Wu, Y. Zhang, and P. Mei, "Structural stability analysis and optimization of the quadrotor unmanned aerial vehicles via the concept of Lyapunov exponents," *The International Journal of Advanced Manufacturing Technology*, vol. 94, no. 9-12, pp. 3217–3227, 2018.

[33] Matlab, *Pixhawk Pilot Support Package (PSP) User Guide*, MathWorks Pilot Engineering Group, 2017.